Effect of Fiber Orientation on Mode I Fracture Toughness of CFRP

Hiroaki Miyagawa,[1]* Chiaki Sato,[2] Kozo Ikegami[2,3]

[1]*Department of Precision Machinery Systems, Interdisciplinary Graduate School of Science and Engineering, Tokyo Institute of Technology, Yokohama 226-8502, Japan*
[2]*Precision and Intelligence Laboratory, Tokyo Institute of Technology, Yokohama 226-8503, Japan*
[3]*Department of Mechanical Engineering, College of Engineering, Tokyo Denki University, Tokyo 101-8457, Japan*

Received 16 November 2007; accepted 11 February 2009
DOI 10.1002/app.30233
Published online 3 November 2009 in Wiley InterScience (www.interscience.wiley.com).

ABSTRACT: The effect of fiber orientations on fracture toughness of carbon fiber reinforced plastics (CFRP) in Mode I loading was investigated using double cantilever beam (DCB) specimens, based on mesoscopic mechanics. Mesoscopic interlaminar fracture toughness of 0//0 interphase of CFRP was evaluated with mesoscopic finite element models using experimental data. The fracture surface roughness was observed by confocal laser scanning microscopy. Then the mesoscopic interlaminar fracture toughness of CFRP was correlated with the fracture surface roughness. Additionally, the change of the Mode I macroscopic fracture toughness of CFRP was experimentally measured with changing the numbers of 0 and $\pm\theta$ layers of DCB specimens. The correlation between the fracture toughness of 0//0 and $\theta//-\theta$ interphases was discussed and a novel procedure was proposed to predict the macroscopic fracture toughness of $\theta//-\theta$ interphase using finite element method (FEM). The fracture toughness of $\theta//-\theta$ interphase analyzed by FEM was finally compared with the experimental results to verify the proposed prediction procedure. © 2009 Wiley Periodicals, Inc. J Appl Polym Sci 115: 3295–3302, 2010

Key words: composites; modeling; orientation; structure–property relations; mesoscopic fracture mechanics

INTRODUCTION

Carbon fiber reinforced plastics (CFRP) have been widely used in the various fields of engineering. The reliability of composite materials against fracture is highly desirable. Primarily, investigations have examined the fracture behavior of unidirectional, quasi-isotropic, and woven reinforced laminates of CFRP from a macroscopic mechanics viewpoint, which regards fiber reinforced composites as completely homogeneous and anisotropic materials[1]; however, multi-directional CFRP have been used for a greater number of structures. Thus, it is important to investigate the behavior of multi-directional laminates made of CFRP. There have been some studies which investigated the fracture behavior of the multi-directional laminates of CFRP.[2–6] All these studies were based on macroscopic mechanics, regarding composite materials as homogeneous.

The great advantage of macroscopic mechanics is the ease to which it is widely applied to all composite materials, based on anisotropic elasticity and linear fracture mechanics. However, the stress and strain values based on the macroscopic mechanics are not real but approximated. Consequently, the real stress and strain values in each multi-directional layer cannot be understood with macroscopic mechanics. On the other hand, mesoscopic mechanics deals with the mechanical behavior of composite materials in the intermediate scale, which is smaller than macroscopic scale as well as larger than molecular scale.[7] The mesoscopic structure of composite materials, including adhesion at matrix/fiber interface, fiber orientation, and fiber geometry, greatly influence the macroscopic properties. When the fiber orientation is changed, the macroscopic mechanical properties of multi-directional CFRP greatly change between specimens. This fact simply leads to the necessity to experimentally investigate fracture toughness of each multi-directional CFRP. Thus, in order to simply predict different fracture toughness of each multi-directional CFRP, it is beneficial to investigate the behavior of multi-directional CFRP based on mesoscopic mechanics, which considers CFRP as a non-homogeneous material, and to give these mesoscopic results to macroscopic mechanics for further investigation. A few studies have investigated the fracture behavior based on mesoscopic mechanics.[8,9] Mostly, the mesoscopic fracture behavior has been analyzed using finite element method (FEM).

**Present address:* Nitto Denko Technical Corporation Oceanside CA 92058, USA
Correspondence to: H. Miyagawa (miyagaw2@msu.edu).

TABLE I
Material Constitutions of DCB Specimens

CFRP	Sequence of layer
DCB specimen A	$[(0)_5//(0)_5]$
DCB specimen B	$[30/-30/30/-30/0//0/-30/30/-30/30]$
DCB specimen C	$[45/-45/45/-45/0//0/-45/45/-45/45]$
DCB specimen D	$[60/-60/60/-60/0//0/-60/60/-60/60]$
DCB specimen E	$[(90)_4/0//0/(90)_4]$
DCB specimen F	$[\theta/(0)_4//(0)_4/\theta]$
DCB specimen G	$[(\pm\theta)_2/(0)_3//(0)_3/(\pm\theta)_2]$
DCB specimen H	$[(\pm\theta)_3/(0)_2//(0)_2/(\pm\theta)_3]$
DCB specimen I	$[\theta/-\theta/\theta/-\theta/\theta//-\theta/\theta/-\theta/\theta/-\theta]$

The present authors have investigated Mode I fracture toughness of multi-directional CFRP based on macroscopic mechanics.[10] In this previous article, the macroscopic strain distribution at the vicinity of the crack tip of multi-directional CFRP was experimentally measured by micro-Raman spectroscopy, and the macroscopic fracture toughness in Mode I was determined from the strain distribution. Additionally, taking an advantage of high resolution of the micro-Raman spectroscopy, the mesoscopic strain distribution of epoxy matrix phase at the vicinity of the crack tip of unidirectional CFRP was experimentally measured by micro-Raman spectroscopy and analyzed using FEM. Then the Mode I fracture toughness of unidirectional CFRP was investigated in more details to find a correlation between macroscopic fracture toughness of CFRP and mesoscopic fracture toughness of epoxy matrix phase.[11,12] However, the effect of the fiber orientation on the fracture toughness of cracked interphase and the correlation between fracture toughness of $0//0$ and $\theta//-\theta$ have not been yet further investigated with applying mesoscopic mechanics to multi-directional CFRP.

Therefore, the effect of fiber orientations on the Mode I fracture toughness of multi-directional CFRP is discussed based on the mesoscopic mechanics in this article. It is shown that the macroscopic fracture toughness of CFRP having only $\pm\theta$ interphases can be predicted by several FEM analyses with experimentally measured macroscopic fracture toughness of unidirectional CFRP. First, the macroscopic fracture toughness of multi-directional CFRP cracking on $0//0$ interphase in both Mode I loading was experimentally measured by conventional double cantilever beam (DCB) testing, and the mesoscopic fracture toughness of $0//0$ interphase for various specimens was analyzed with FEM using the experimental data. The change of the mesoscopic fracture toughness of $0//0$ interphase was secondly correlated with the fracture surface roughness measured by confocal laser scanning microscopy. Additionally, the change of the Mode I macroscopic fracture toughness of CFRP was analyzed by FEM with changing the numbers of (0) and ($\pm\theta$) layers of DCB specimens. A novel procedure was proposed to predict the macroscopic fracture toughness of CFRP having only $\pm\theta$ interphases using FEM, while also addressing the relation between $0//0$ and $\theta//-\theta$ interlaminar fracture toughness. This novel approach using FEM provides benefit to predict macroscopic fracture toughness of multi-directional CFRP having only $\pm\theta$ interphases with minimal experiment for a unidirectional CFRP specimen.

EXPERIMENTAL

Materials and specimen preparation

DCB specimens of unidirectional and multi-directional CFRP (T300/#2500, Toray Industry Inc., Japan) were used for fracture testing. Layer sequences of the DCB specimens are shown in Table I. A Teflon film having a thickness of 40 μm with a mold-release agent was employed in order to set an initial crack at the interphase represented as "//" in Table I. Configurations of the DCB specimens are shown in Figure 1. Crack length, specimen width, and specimen thickness are labeled as a, B, and $2h$, respectively. Nominal dimensions of all DCB specimens were $20 < a < 70$ mm, $B \approx 12$ mm, and $2h \approx 2.0$ mm. The DCB specimens were prepared with prepreg laminates that were cured by vacuum bagging in an atmospheric pressure at 130°C for 2 h. Sides of the DCB specimens were cut with a diamond table saw to obtain uniform specimen width and to observe crack length with optical microscopy. Finally, hinges were adhesively bonded at the edge of the DCB specimens as illustrated in Figure 1.

Testing procedure

DCB testing

It is necessary to measure critical load P_C applied to the DCB specimen, crack length a, and crack opening displacement (COD) to evaluate macroscopic

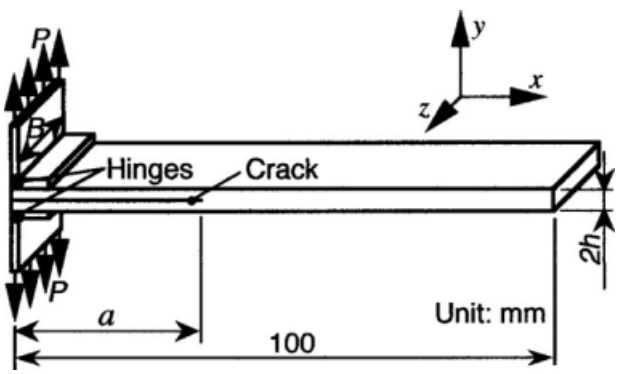

Figure 1 Dimensions of DCB specimens for Mode I fracture testing.

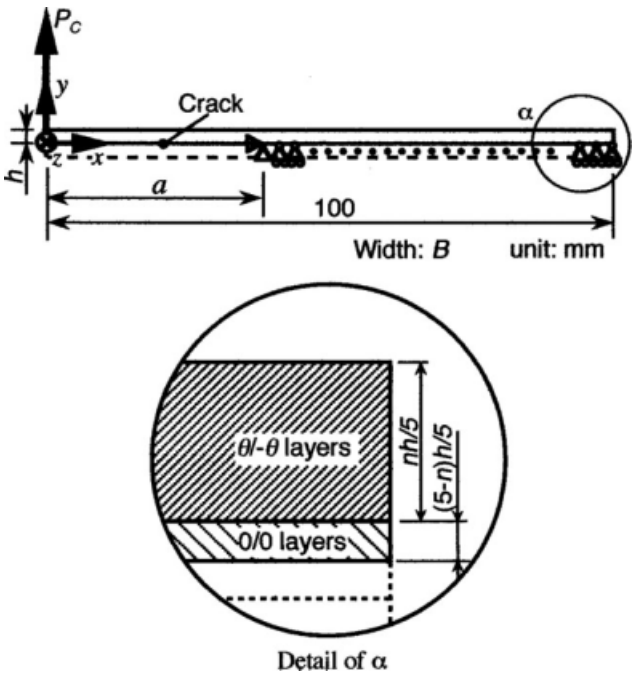

Figure 2 Dimensions of mesoscopic FEM model for DCB specimens.

fracture toughness. The crack length was measured on one side of the DCB specimen by an optical microscope while the DCB specimens were moved on the *x-y* stage. The conventional DCB experiments were performed with a crosshead velocity of 0.5 mm/min for loading the specimens. The COD was calculated from the crosshead travel with correcting for compliance of the load cell.

Fractographic observations

2-D fracture surface profiles of 0//0 interphase of the multi-directional DCB specimens were acquired in a range of 135 μm width using Keyence VF-7000 confocal laser scanning microscope (CLSM) with a 100× magnification and a He-Ne laser of 632.8 nm wavelength. The surface profiles were scanned perpendicularly to the carbon fibers (direction of crack propagation) at 10 random locations to determine the arithmetical mean deviation of the profile R_a.

Fracture surfaces of DCB specimens were observed by Hitachi S-3500N scanning electron microscope (SEM) at 10 kV accelerating voltage, after the fracture surfaces of the DCB specimens were sputter-coated with Au/Pd thin films.

FINITE ELEMENT ANALYSIS

A 2-D mesoscopic FEM model of the DCB specimen, shown in Figure 2, was analyzed to investigate mesoscopic fracture toughness of the cracked 0//0 and the θ//−θ interphases in both Mode I loading. Half of the DCB specimens were modeled for FEM analysis since the deformation is symmetric in pure Mode I loading. In this mesoscopic FEM model, unidirectional and (±θ) layers are distinctive. The mechanical properties used in the analysis for each layer are shown in Table II. The crack was located at the center of the specimen. Ten triangular singular elements were located at the crack tip of the DCB specimens. Most importantly, the area in the vicinity of the crack tip was precisely meshed with triangular elements having six nodes. All element size was less than the half of the thickness of 0/0 and ±−θ layers in Figure 2. It has been confirmed that the FEM models with this element size provided the same results as those with smaller element size. The experimental critical load P_C for each DCB specimen was applied in the FEM analysis. The load P_C was applied perpendicularly to the specimen as shown in Figure 2. The FEM model was analyzed in a plane stress state. Since these models were analyzed based on mesoscopic mechanics, the mesoscopic fracture toughness of the layers where the crack existed could not be determined using virtual crack extension method. Therefore, stress direct method was utilized to evaluate the mesoscopic fracture toughness of cracked interphases. No residual stress of individual layers was considered in all FEM analysis to analyze the mesoscopic fracture toughness.

RESULTS AND DISCUSSION

DCB testing

The macroscopic fracture toughness K_{IC} of Specimens A–E in Mode I was evaluated from the load–displacement diagram by modified compliance calibration (MCC) method.[13] Plastic behavior was not observed until crack propagation in the cases of Specimens A and B. This meant that the stress was

TABLE II
Mechanical Properties for Oriented Layers of CFRP

CFRP	E_x (GPa)	E_y (GPa)	E_z (GPa)	v_{xy}	v_{xz}	v_{yz}	G_{xy} (GPa)	G_{xz} (GPa)	G_{yz} (GPa)
$(0/0)_s$	117	8.54	8.54	0.278	0.278	0.500	3.90	3.90	2.83
$(30/-30)_s$	37.8	8.54	9.11	0.277	1.40	0.367	3.56	23.6	3.04
$(45/-45)_s$	12.5	8.54	12.5	0.323	0.825	0.221	3.28	29.1	3.28
$(60/-60)_s$	9.11	8.54	37.8	0.392	0.338	0.0625	3.04	23.6	3.56
$(90/-90)_s$	8.54	8.54	117	0.500	0.0203	0.0203	2.83	3.90	3.90

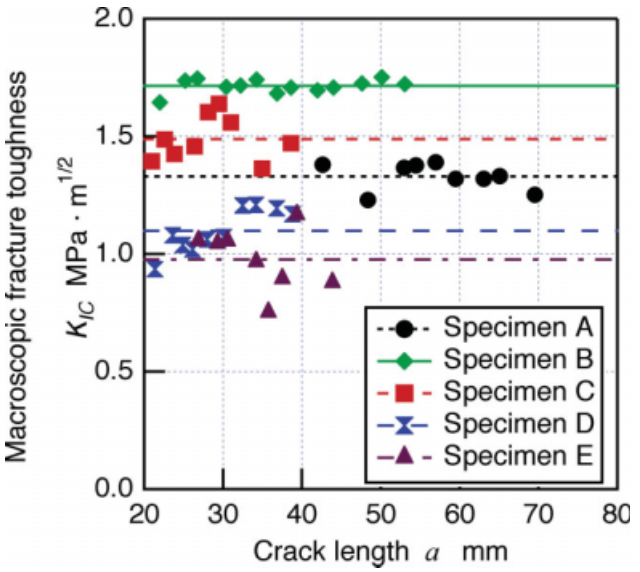

Figure 3 Mode I macroscopic fracture toughness of all multi-directional DCB specimens having a crack on 0//0 interphase. [Color figure can be viewed in the online issue, which is available at www.interscience.wiley.com.]

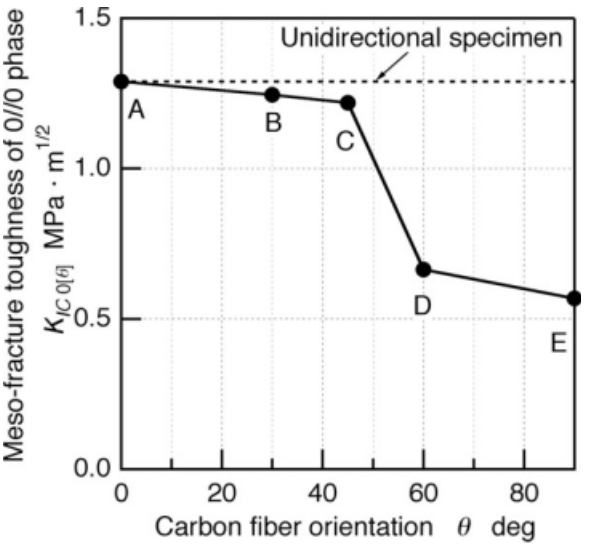

Figure 4 Relation between fiber orientation and mesoscopic fracture toughness of 0//0 interphase analyzed by FEM for Specimens A–E.

well transferred to reinforcement carbon fibers for Specimens A and B due to their small angles of fiber orientation. In other words, less stress was loaded to epoxy matrix, and the crack was propagated in the epoxy matrix phase before the matrix started to show plastic deformation. In this case, the maximum load was used as the critical load P_C to determine critical energy release rate and fracture toughness. On the other hand for Specimens C–E, it was difficult to determine the maximum load because of the plastic behavior. This meant that the stress was not well transferred to reinforcement carbon fibers for Specimens C–E due to their large angles of fiber orientation, and more stress causing plastic deformation was loaded to epoxy matrix. In this case, the load at the intersection point of load-COD line and 5% offset line was regarded as the critical load P_C. Figure 3 shows the results of the Mode I macroscopic fracture toughness K_{IC} for different crack lengths evaluated by MCC. No clear increase of the macroscopic fracture toughness depending on different crack lengths was observed in Figure 3. The average values of the macroscopic fracture toughness regardless of different crack lengths is shown in Figure 3 as solid and broken lines for reference. The deviation of the macroscopic fracture toughness was within 10% for all DCB specimens. Since all crack propagated along the fiber orientation on 0//0 interphase and no transverse crack onto other interphases was observed, the crack propagation was consistent and minimal deviation of the macroscopic fracture toughness was caused. The maximum average value of the macroscopic fracture toughness was achieved with 30° fiber orientation, and then it started to decrease with increasing the angle of fiber orientation. This suggests that the macroscopic fracture toughness can increase with increasing the angle of fiber orientation while the multi-directional CFRP have some certain level of stiffness and the deformation of epoxy matrix is still elastic. Once the epoxy matrix shows the plastic behavior with larger angles of fiber orientation, the macroscopic fracture toughness starts to decrease with decreasing elastic modulus of multi-directional CFRP.

Mesoscopic fracture toughness of 0//0 interphase

Figure 4 shows the Mode I mesoscopic fracture toughness $K_{IC0[\theta]}$ of 0//0 interphase, analyzed by FEM for the DCB Specimens A–E. The specimen data shown in Table III were utilized for the mesoscopic FEM analysis. The mesoscopic fracture toughness of 0//0 interphase decreased with increasing the angle of fiber orientation. The residual stress due to asymmetry in the sub-beam could cause a reduction of the mesoscopic fracture toughness of 0//0

TABLE III
Dimensions of DCB Specimens used for the Mesoscopic FEM Analysis

CFRP	Critical load, P_C (N)	Crack length, a (mm)	Specimen width, B (mm)	Specimen thicnkess, $2h$ (mm)
Specimens A	10.1	48.4	13.2	0.967
Specimens B	9.60	36.9	13.2	0.965
Specimens C	8.14	28.1	12.4	0.973
Specimens D	3.87	28.0	11.6	0.950
Specimens E	3.03	34.2	13.2	0.973

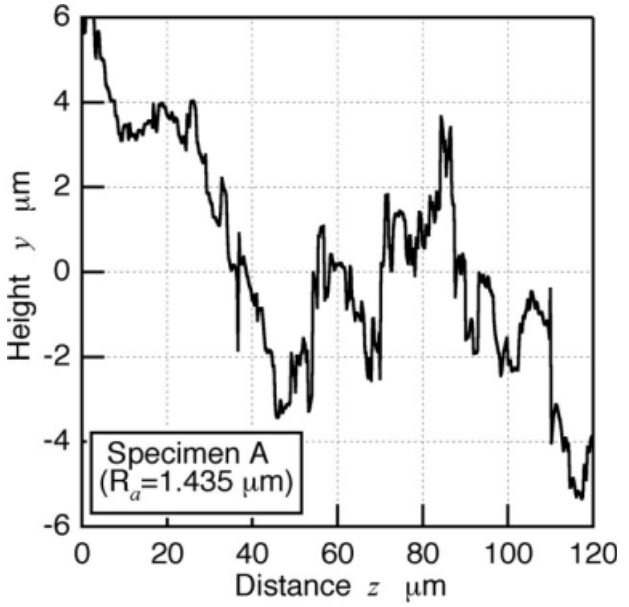

Figure 5 An example of fracture surface profile of Specimen A.

interphase for Specimens C–E. In other words, the homogeneity of the residual stress in all five layers of the sub-beam of the DCB specimens was not obtained; this fact resulted in the larger residual stress in the 0//0 layers after curing. The shrinkage along the fiber orientation was smaller than that perpendicular to the fiber orientation, since carbon fibers have much lower coefficient of thermal expansion than epoxy matrix in general and not carbon fibers but epoxy matrix will shrink during curing process. Indeed, the large permanent crack opening was observed especially for Specimens D and E. Therefore, the tensile residual stress along y-axis existed in 0//0 interphase for Specimens B–E. If residual stress of Specimens D and E were minimized, the macroscopic fracture toughness of these specimens would have been higher in Figure 3. This decreased mesoscopic fracture toughness in 0//0 interphase may also imply that the increase of the macroscopic fracture toughness of multi-directional CFRP specimens is possible with designing the layer sequence to cause compressive residual stress on the cracked interphase.

Figure 5 shows an example of fracture surface profile line measured by CLSM. The arithmetical mean deviation of profile R_a was calculated from each profile line. Figure 6 shows the correlation between R_a and the mesoscopic fracture toughness $K_{IC0[\theta]}$ of 0//0 interphase for Specimens A–F shown in Figure 4. It was obvious that the surface roughness increased with decreasing the mesoscopic fracture toughness of 0//0 interphase of the DCB specimens. Furthermore, another observation using SEM also revealed that the interphase crack was propagated at the interface of reinforcement carbon fibers and epoxy matrix especially for Specimens D and E. Hence, the residual stress lessened the interface strength.

Fracture toughness of θ//−θ interphase

The macroscopic fracture toughness is dependent on the fiber orientations, though the same materials are used as polymer matrix and reinforcement fibers with the same volume fraction. The macroscopic fracture toughness can be calculated once the elastic moduli, specimen size, crack length, compliance, and the critical load are known. Arbitrary values can be used for the crack length and the specimen size in FEM models, assuming that each CFRP specimen has a constant fracture toughness, regardless of crack length and specimen size. The macroscopic elastic moduli of an arbitrary sequence of layers can be calculated from Table II with the laminate theory. The compliance is calculated from the crack length, the specimen size, and the elastic moduli. Consequently, understanding the critical load is crucial in determining the macroscopic fracture toughness.

Figure 7 shows a proposed procedure to predict the macroscopic fracture toughness of arbitrary multi-directional CFRP. Assuming that the multi-directional CFRP do not have significant residual stress, this procedure in Figure 7 allows predicting the macroscopic fracture toughness of arbitrary multi-directional CFRP using only simple 2-D FEM analyses and the experimental results of unidirectional CFRP. In the first step, it is necessary to experimentally measure the macroscopic fracture toughness of the unidirectional CFRP specimen. In

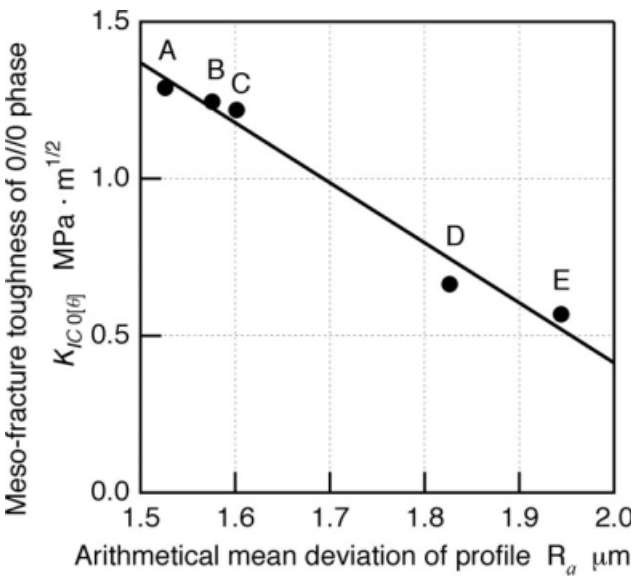

Figure 6 Correlation between surface roughness and mesoscopic fracture toughness of 0//0 interphase in Mode I.

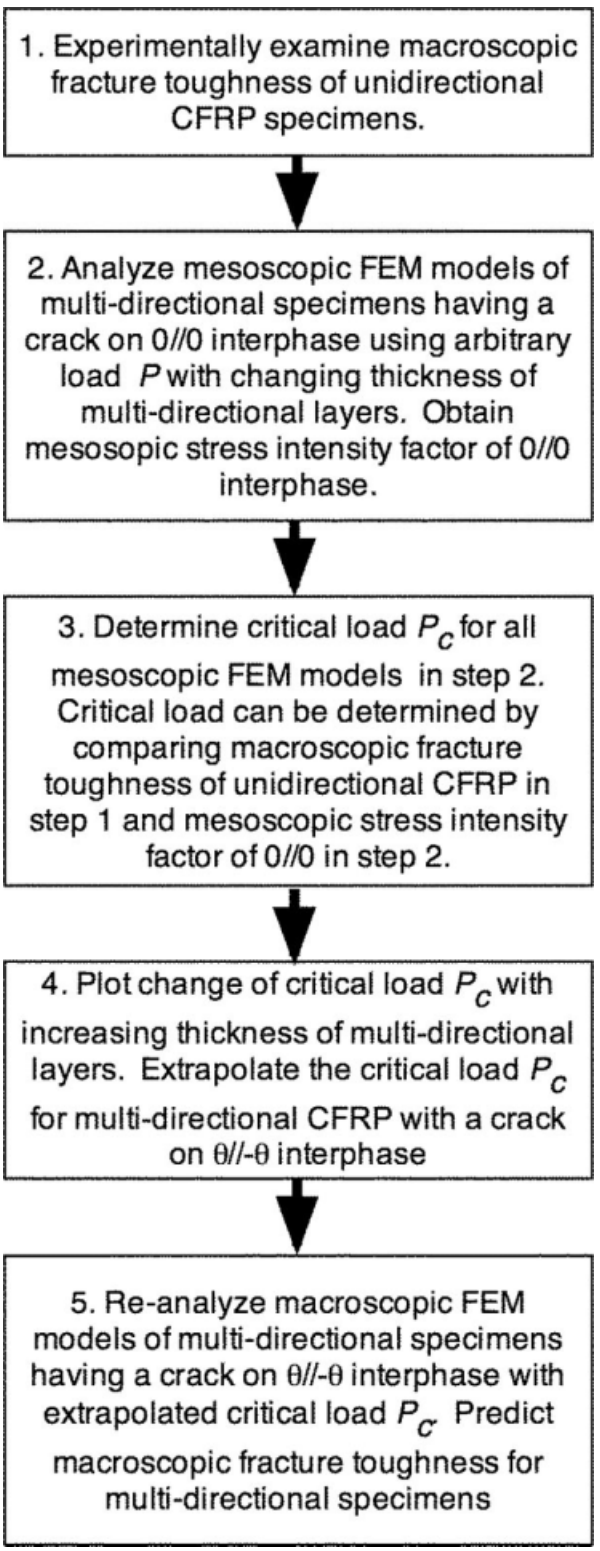

Figure 7 Procedure for predicting macroscopic fracture toughness of multi-directional CFRP.

the second step, mesoscopic FEM models of multi-directional specimens having a crack on 0//0 interphase, as shown in Figure 2, are analyzed using an arbitrary load value P with changing thickness of multi-directional layers. The mesoscopic stress intensity factor of 0//0 interphase can be obtained in this analysis step. In the third step, critical load P_C for all mesoscopic FEM models used in step 2 is determined. Critical load P_C can be determined by comparing macroscopic fracture toughness of unidirectional CFRP obtained in step 1 and mesoscopic stress intensity factor of 0//0 interphase obtained in step 2, since the macroscopic fracture toughness for unidirectional CFRP and the mesoscopic fracture toughness of 0//0 interphase of multi-directional CFRP must be the same and the relation between load and stress intensity factor is proportional. Once the change of critical load P_C with increasing thickness of multi-directional layers in Figure 2 is plotted on the figure, the critical load P_C for multi-directional CFRP with a crack on θ//−θ interphase can be extrapolated by curve fitting, assuming that the crack propagation condition is the same regardless of fiber orientation on the cracked interphase. Finally a macroscopic FEM model (where specimen dimensions are exactly the same as the mesoscopic model in step 2), assuming that CFRP are homogeneous, of multi-directional CFRP specimens having a crack on θ//−θ interphase is analyzed with the extrapolated critical load P_C. The obtained stress intensity factor is regarded as the macroscopic fracture toughness since the critical load is the applied load in the macroscopic model. At last, this procedure for prediction of the macroscopic fracture toughness of multi-directional specimens is completed. If necessary, the macroscopic critical energy release rate can be converted from the macroscopic fracture toughness.

The change of the critical load with increasing number n of (±θ) layers of DCB Specimens F–H was analytically investigated by FEM as Figure 7. In this analysis the effect of residual stress was neglected. The FEM analyses were conducted with the values of $h = 1.0$ mm, $a = 30$ mm, and $P = 10$ N for the DCB specimens. A value of the Mode I macroscopic fracture toughness of unidirectional CFRP used in this analysis was 1.3 MPa $m^{1/2}$ as shown in Figure 3. Figure 8 shows the change of the critical load for the fiber orientations of ±30°, ±45°, and ±60°. In Figure 8, critical load in Mode I loading with respect to the number n of oriented layers became minimum with Specimen H ($n = 3$), regardless of fiber orientations. In Figure 8, the 2nd-rate equation seems to fit with the analyzed results for the least-squares curve fit; however, the mechanical meaning of this curve fit is not yet clear. Assuming that the crack on θ//−θ interphase propagates in the same condition as that of 0//0 interphase, then the critical load P_C was extrapolated for Specimen I for all fiber orientations.

With the extrapolated critical load P_C, the macroscopic fracture toughness of Specimen I was predicted as shown in Figure 9. The analyzed

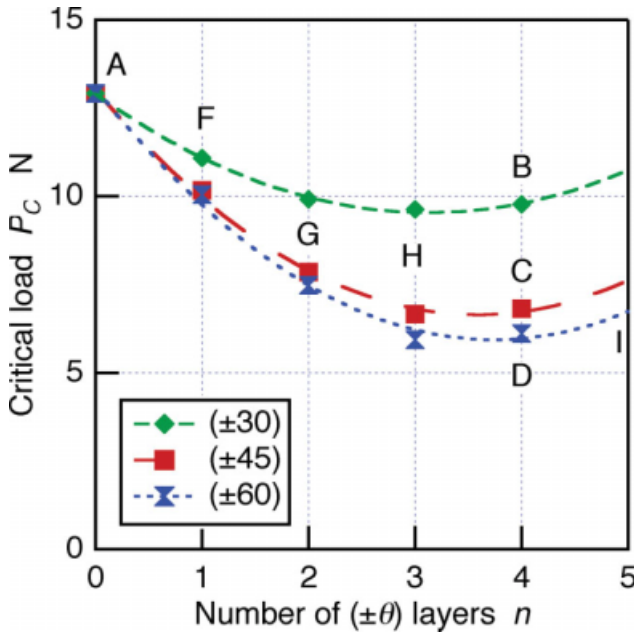

Figure 8 Change of critical load analyzed by FEM with changing the number of (±θ) layers. [Color figure can be viewed in the online issue, which is available at www.interscience.wiley.com.]

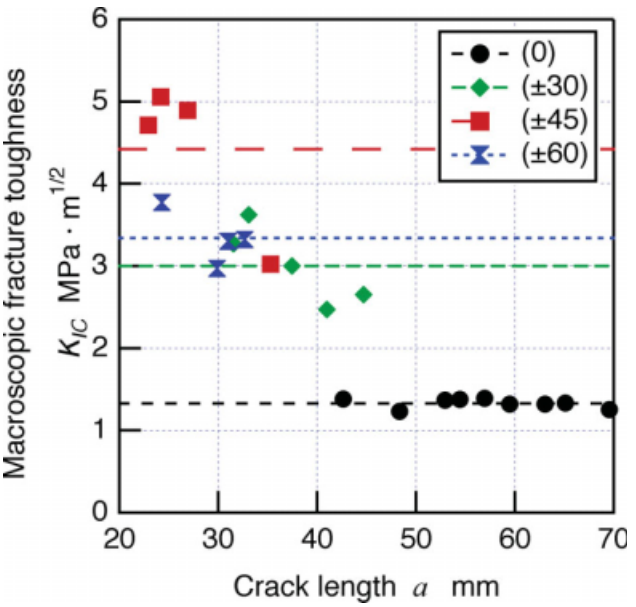

Figure 10 Mode I macroscopic fracture toughness of all multi-directional DCB Specimen I having a crack on θ̃//θ interphase. [Color figure can be viewed in the online issue, which is available at www.interscience.wiley.com.]

macroscopic fracture toughness increased by increasing the fiber orientation angle to 45° and remain the same with the fiber orientation angle of 60°. In order to verify this proposed prediction procedure, the macroscopic fracture toughness for Specimen I with the fiber orientations of ±30°, ±45°, and ±60° was experimentally measured by MCC method. The fracture toughness of these specimens with different crack lengths are shown in Figure 10, while Figure 9 shows average values that may be compared with analytical results. The experimental macroscopic fracture toughness was higher than predicted for all fiber orientation angles. The macroscopic fracture toughness K_{IC} of the unidirectional (0°) CFRP showed the lowest value, and that of the multi-directional CFRP was maximized in Figure 7, when the fiber orientation is ±45°.

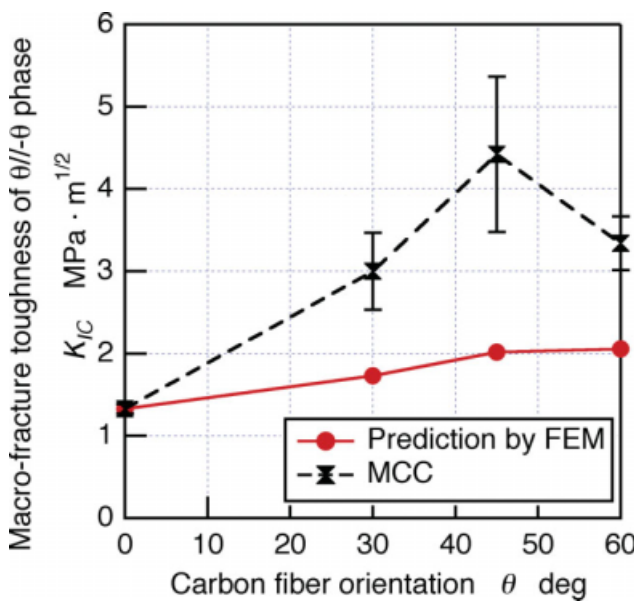

Figure 9 Prediction by FEM and experimental results of the macroscopic fracture toughness of DCB Specimen I having a crack on θ̃-θ interphase. [Color figure can be viewed in the online issue, which is available at www.interscience.wiley.com.]

The gap between experimental and analyzed results in Figure 10 can be discussed with SEM micrographs. When the fracture surfaces of these multi-directional DCB specimens were observed by SEM, it was easily found in low magnification that the crack transversely moved to the different interphase for all multi-directional DCB specimens. The non-central position of the transverse crack resulted in crack propagation in the mixed Mode (I + II). The present authors have previously reported the macroscopic fracture toughness and the morphologies of the fracture surface of 0//0 interphase in pure Mode I, II, and III.[14] The macroscopic fracture toughness in Mode II loading was much higher than that in Mode I loading. The fracture surface morphology of unidirectional CFRP in Mode I loading was generally flat and wholly covered with resin. On the other hand, as a characteristic of the fracture surface in Mode II, many uneven facets of resin, called hackles, were widely observed throughout the surface of unidirectional CFRP, and the reinforcement fibers were strikingly exposed. Figure 11 shows examples of

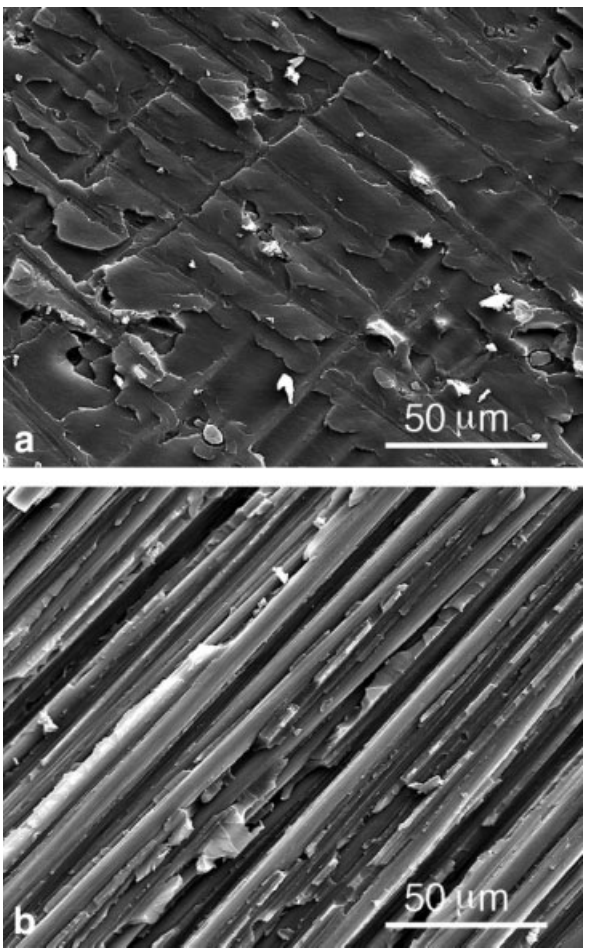

Figure 11 SEM micrographs showing two different morphologies of fracture surface of 45//−45 interphase in Mode I loading (a) Before the transverse crack propagation (b) After the transverse crack propagation.

fracture surfaces for Specimen I with the fiber orientation of ±45° before and after the crack transversely moved to the different interphase. In Figure 11(a), the fracture surface seems to be flat, and the reinforcement fibers are wholly covered with epoxy matrix (characteristic of pure Mode I fracture surface). However in Figure 11(b), the reinforcement carbon fibers are exposed, and this morphology seems similar to that in Mode II loading. Considering that the macroscopic Mode II fracture toughness of the unidirectional CFRP was greater than the macroscopic Mode I fracture toughness; the macroscopic Mode I fracture toughness of multi-directional DCB specimens became higher than predicted, because of the non-centered transverse crack. Additionally, it can be expected that the transverse crack also provides an effect as "fiber-bridging." The effects of transverse crack and fiber bridging have not been considered in the FEM analyses. Thus, the multi-directional interphase has a better tolerance against the crack propagation versus the 0//0 interphase in Mode I loading. Although the ratio of the mixed Mode (I + II) and the accurate increased value of the macroscopic fracture toughness could not be predicted, the procedure in Figure 7 is still useful with providing safer (lower) estimated values of macroscopic fracture toughness of multi-directional CFRP.

CONCLUSIONS

The fracture toughness of multi-directional CFRP was investigated based on mesoscopic fracture mechanics. The mesoscopic fracture toughness of 0//0 interphase was determined using simple mesoscopic analyses using FEM, with distinguishing different fiber orientations. The fracture surface roughness was observed by CLSM, and the relation between the mesoscopic fracture toughness of 0//0 interphase and the fracture surface roughness was correlated with the residual stress caused by the asymmetry of the layer sequence of the DCB specimens. A novel procedure was proposed to predict the macroscopic fracture toughness of CFRP having ±θ interphases using an experimental value of the macroscopic fracture toughness of unidirectional CFRP and simple mesoscopic analyses using FEM. The $\tilde{\theta}//\theta$ interphase provided better tolerance to the crack propagation versus 0//0 interphase in Mode I loading, and consequently the experimental results showed a higher fracture toughness than predicted by FEM. The reason for the higher fracture toughness from experimental results was also confirmed by the fracture surface morphologies observed by SEM.

References

1. Wilkins, D. J.; Eisenmann, J. R.; Camin, R. A.; Margolis, W. S.; Benson, R. A. In Damage in Composite Materials, ASTM Special Technical Publication 775; Reifsnider, K. L., Ed.; American Society for Testing and Materials: Philadelphia, 1980; pp 168–183.
2. Nicholls, D. J.; Gallagher, J. P. J Reinforced Plast Compos 1983, 2, 2.
3. Chai, H. Composites 1984, 15, 277.
4. Laksimi, A.; Benzeggagh, M. L.; Jing, G.; Hecini, M.; Roelandt, J. M. Composite Sci Technol 1991, 41, 147.
5. Robinson, P.; Song, D. Q. J Compos Mater 1992, 26, 1554.
6. Chou, I.; Kimpara, I.; Kageyama, K.; Ohsawa, I. In Composite Materials: Fatigue and Fracture, ASTM Special Technical Publication 1230; Martin, R. H., Ed.; American Society for Testing and Materials:Philadelphia, 1995; Vol. 5, pp 132–151.
7. Chamis, C. C.; Gotsis, P. K. J Thermoplast Compos Mater 1998, 11, 478.
8. Nairn, J. A. J Compos Mater 1989, 23, 1106.
9. Kimachi, H.; Tanaka, H.; Tanaka, K. JSME Int J Ser A 1999, 42, 537.
10. Miyagawa, H.; Sato, C.; Ikegami, K. Compos Sci Technol 2000, 60, 2903.
11. Miyagawa, H.; Sato, C.; Ikegami, K. Mech Mater 2002, 34, 179.
12. Miyagawa, H.; Sato, C.; Ikegami, K. SAMPE J 2000, 38, 7.
13. Kageyama, K.; Chou, T. W. Composites 1987, 18, 393.
14. Miyagawa, H.; Sato, C.; Ikegami, K. Appl Compos Mater 2001, 8, 25.